Article

Cite This: Biomacromolecules 2018, 19, 1435−1444

pubs.acs.org/Biomac

Influence of Grafted Block Copolymer Structure on Thermoresponsiveness of Superparamagnetic Core−Shell Nanoparticles

Steffen Kurzhals,[†] Martina Schroffenegger, Noga Gal, Ronald Zirbs, and Erik Reimhult*

Institute for Biologically Inspired Materials, Department of Nanobiotechnology, University of Natural Resources and Life Sciences, Vienna, Muthgasse 11, 1190 Vienna, Austria

Supporting Information

ABSTRACT: The morphology and topology of thermoresponsive polymers have a strong impact on their responsive properties. Grafting onto spherical particles has been shown to reduce responsiveness and transition temperatures; grafting of block copolymers has shown that switchable or retained wettability of a surface or particle during desolvation of one block can take place. Here, doubly thermoresponsive block copolymers were grafted onto spherical, monodisperse, and superparamagnetic iron oxide nanoparticles to investigate the effect of thermal desolvation on spherical brushes of block copolymers. By inverting the block order, the influence of core proximity on the responsive properties of the individual blocks could be studied as well as their relative influence on the nanoparticle colloidal stability. The inner block was shown to experience a stronger reduction in transition temperature and transition enthalpy compared to the outer block. Still, the outer block also experiences a significant reduction in responsiveness due to the restricted environment in the nanoparticle shell compared to that of the free polymer state. The demonstrated pronounced distance dependence importantly implies the possibility, but also the necessity, to radially tailor polymer hydration transitions for applications such as drug delivery, hyperthermia, and biotechnological separation for which thermally responsive nanoparticles are being developed.

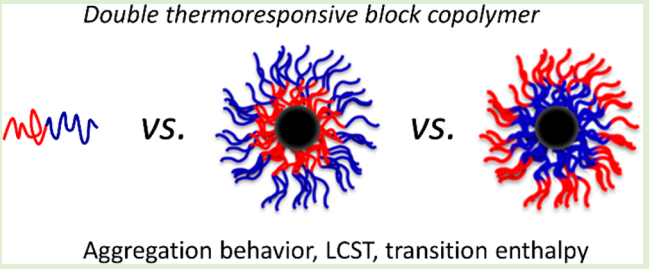

INTRODUCTION

Thermoresponsive core−shell nanoparticles are an interesting class of materials due to their externally controlled reversible dispersibility.[1−4] Combining a thermoresponsive shell with a magnetic core such as biocompatible, superparamagnetic iron oxide nanoparticles (SPIONs) is especially beneficial as it allows for (magneto)thermal heating and extraction useful for a broad spectrum of applications, including water desalination,[5] contrast agents,[6] nanothermometers,[6,7] catalysis,[8] and biomedical agents for hyperthermia[9] or drug delivery.[10,11] An important limitation in designs for biomedical and biotechnological applications has been that magnetothermal actuation of magnetic nanoparticles has been limited to changing the bulk temperature to change particle properties or colloidal aggregate size. This is due to the quite simple design of linear homo- or random copolymer used so far to graft thermoresponsive brushes as shells. Although magnetic heating proceeds from the core, the thermal conductivity (heat dissipation) of water is so high that a large temperature gradient over tens of nanometers cannot be supported. On the other hand, high colloidal stability and reversible nanoparticle aggregation require polymer shells of such thickness, and the polymer solubility transition extends over several degrees Kelvin. For a shell with uniform transition temperature, it is therefore difficult to envision how simultaneous colloidal stability and colloidal transitions through heating from the core should be accomplished.

Improved design of these materials for specific purposes therefore requires better understanding of the impact of grafting on the responsive behavior of the polymeric dispersant comprising the shell as this will define the final material properties, such as colloidal aggregation and deaggregation with respect to application temperature and other solvent conditions. The impact of grafting on thermoresponsive properties of homopolymers and random copolymers has been investigated. The influence of polymer molecular weight (MW) of grafted poly(*N*-isopropylacrylamide) (PNIPAM) was described recently, showing strong reduction of transition enthalpy compared to free polymers with decreasing molecular weight.[12] This loss in transition enthalpy correlates with a reduction in aggregate size, preventing (magneto)thermal extraction of the material that depends on formation of large superparamagnetic core aggregates.[12] Reduction in enthalpy was also observed for grafting of polyoxazoline homo- and random copolymers.[13] In that particular study, incorporation of ethyl-oxazoline units led to a significant reduction in transition

Special Issue: Stimuli-Sensitive and -Responsive Polymer Biomaterials

Received: September 28, 2017
Revised: November 18, 2017
Published: November 21, 2017

DOI: 10.1021/acs.biomac.7b01403
Biomacromolecules 2018, 19, 1435−1444

enthalpy compared to a pure poly(2-isopropyloxazoline) (PIPOx) brush and to even stronger reduction compared to that for free polymers.[13] Interestingly, although grafting of PNIPAM had little effect on the transition temperature,[3,12] a reduction was observed for other thermoresponsive polymer brushes such as polyoxazolines,[13,14] polypeptoids,[4] and poly(poly(ethylene glycol) methacrylate)[15] compared to their free polymer analogues.

An important question that remains for further design of optimized responsive brush shells is how different segments in the brush are affected by the grafting process; for example, do only inner chain segments experience a loss in responsiveness and a significant shift in critical solution temperature while outer chain segments remain unaffected? The segment density close to the core of the densely grafted brush is very high. Hence, one could argue that the expected effect on the desolvation transition would be even higher on this part of the polymer than the well-described effect of increasing the molecular weight of a polymer coil. Conversely, at least for high molecular weight-grafted polymers on a highly curved nanoparticle surface, the outer shell polymer density could be similar to that of individual free coils of lower molecular weight and experience no or converse changes in the desolvation transition compared to free polymer of the same molecular weight. For accessing and investigating different regimes in a spherical brush, an approach using block copolymers could be advantageous as it allows us to tune the distance of the thermoresponsive segment to the core via sequential living polymerization. One can envision that optimized designed sequences of polymer blocks and thereby transition temperatures could allow control of the colloidal transition by, e.g., magnetic heating from the core alone.

Aggregation of thermoresponsive ABA-type[16−18] and ABC-type triblock copolymers[19−24] into soft−soft core−shell nanoparticles has been studied, which could provide a guide to the expected responsive behavior of hard core−polymer shell nanoparticles. Although most often only one thermoresponsive block is present in the corona, doubly thermoresponsive triblock PS-*b*-PNIPAM-*b*-(oligoPEG PS) micelles were described by Zhang and co-workers.[24] After formation of the PS core, the shell can be collapsed stepwise. Heating above the first critical solution temperature (CST) leads to collapse of the inner PNIPAM block. The outer oligo-PEGylated PS block collapses above the second CST, which is visible in a further reduction in size at first before ultimately the core−shell nanoparticles aggregate into larger clusters. Examples of similar studies on thermoresponsive block copolymers grafted onto inorganic nanoparticles are rare.[25,26] Thermoresponsive gold nanoparticles Au@PNIPAM-*b*-PMMA (PNIPAM MW 40 kDa) were reported by Tang.[26] Analogously to the described triblock copolymers, collapse of the inner block resulted in a drop in size of 19 nm, which was reversible upon cooling. However, no study yet described the influence of core proximity on the responsive properties of a grafted polymer brush or aggregation of doubly thermoresponsive nanoparticles.

Thus, we present a model system based on block copolymer-modified SPION to explore the impact of core proximity on inner and outer segments of a spherical brush with respect to morphology, aggregation behavior, transition temperature, and enthalpy.

EXPERIMENTAL SECTION

MATERIALS

All chemicals were purchased from Sigma-Aldrich unless otherwise noted. Oleic acid-coated SPION were prepared by thermal decomposition of iron(0)pentacarbonyl in dioctyl ether in the presence of oleic acid.[27,28] 6-Nitrodopamine hydrogensulfate was prepared as reported previously.[27,28] 2-Isopropyloxazoline (IPOx) was prepared by condensation of 2-aminoethanol with isobutyronitrile using zinc acetate as catalyst,[29] dried over calcium hydride, and distilled at reduced pressure. ^{1}H NMR ($CDCl_3$, δ, ppm): 4.25 (2H, t, ^3J = 9.4 Hz), 3.84 (2H, t, ^3J = 9.4 Hz), 2.61 (1H, sep, ^3J = 7.0 Hz), 1.19 (6H, d, ^3J = 7.0 Hz).

2-Ethyloxazoline (EtOx, ≥99%) and *N*,*N*-diisopropylethylamine (DIPEA, 99.5%) were dried over calcium hydride and distilled at reduced pressure. Methyl tosylate (MeTos, 98%) was purified by distillation. *N*,*N*-Dimethylacetamide (DMA, anhydrous, 99.8%) was purchased from Sigma-Aldrich. COMU: (1-cyano-2-ethoxy-2-oxoethylidenaminooxy) dimethylamino-morpholino-carbenium hexafluorophosphate. DMAP: 4-(dimethylamino)pyridine. Dialysis tubes (molecular weight cut-off (MWCO): 3.5 kDa (regenerated cellulose) and 1000 kDa (cellulose ester, Spectra/Por Float-A-Lyzer)) were purchased from Carl Roth.

Polymerization. Example polymerization for HO-PEtOx-*b*-PIPOx: polymerization reactions were performed in a Glovebox (GS Glovebox Systemtechnik GmbH) with water-level <1 ppm and oxygen-level <5 ppm. A screwcap vial equipped with a magnetic stir bar was charged with 2-isopropyloxazoline (0.5 mL, 0.42 mmol) and anhydrous DMA (2.7 mL). The flask was placed in a preheated oil bath at 100 °C. The polymerization was started by adding a solution of methyl tosylate in DMA (246 μL (stock solution: 0.1 mL of methyl tosylate in 3 mL of DMA), 0.053 mmol). After 20 h, 2-ethyloxazoline (0.42 mL, 4.2 mmol) was added, and the polymerization was continued for another 20 h. The reaction was quenched by addition of water (3 drops) and stirred overnight. The polymer was precipitated by dropping the reaction solution into hexane/diethyl ether (v/v: 4/1), collected by centrifugation, and dried in vacuo. Yield: 900 mg (90%), GPC (*N*,*N*-dimethylformamide (DMF) with LiBr (0.05 M)): 19.4 kDa, Đ = 1.2.

Carboxyl-Terminated Polyoxazoline. A solution of hydroxy-terminated block copolymer (900 mg, 0.047 mmol), succinic anhydride (45 mg, 0.45 mmol), and DMAP (18 mg, 0.15 mmol) in toluene (10 mL) was refluxed for 24 h. After cooling to room temperature, the product was precipitated in hexane/diethyl ether (v/v: 4/1). The polymer was collected via centrifugation and dried in vacuo. Yield: 700 mg (70%).

Nitrocatechol-Terminated Polyoxazoline. Carboxyl-terminated polyoxazoline (700 mg, 0.036 mmol), COMU (40 mg, 0.093 mmol), and DIPEA (50 μL) in DMF (5 mL) were reacted for 10 min at 0 °C to activate the polymer. A solution of 6-nitrodopamine hydrogensulfate (38 mg, 0.12 mmol) in DMF (1 mL) was added, and the reaction solution was stirred for 3 days at room temperature. The solution was dropped into hexane/diethyl ether (v/v: 4/1) to precipitate the polymer. The yellow residue was washed with hexane, air-dried, and dissolved in Milli-Q water. The aqueous solution was dialyzed (3.5 kDa membrane cut-off size) to remove free nitrodopamine and reaction byproducts. The polymer was obtained after freeze-drying (450 mg). ^{1}H NMR for PIPOx-*b*-PEtOx-NDA ($CDCl_3$, δ, ppm): 7.61 (s, 1H, Ar−H), 6.74 (s, 1H, Ar−H), 4.20 (2H, CH_2OCO−), 3.45 (4nH, -*N*−CH_2CH_2- PIPOx, PEtOx), 2.65−2.89 (1nH, $CH(CH_3)_2$, PIPOx), 2.28−2.39 (2nH, CH_2CH_3, PEtOx), 1.09 (6nH, $CH(CH_3)_2$, PIPOx, 3mH, CH_2CH_3, PEtOx).

Grafting-to" Reaction. As prepared, oleic acid-coated SPION (9.8 ± 0.6 nm, 100 mg) and nitrocatechol-terminated polyoxazoline (450 mg) were suspended in DMF (5 mL) and reacted under ultrasonication for 24 h. The solution was dropped into hexane/diethyl ether (v/v: 4/1) to precipitate the raw product. The brown residue was washed with hexane and air-dried. The core−shell nanoparticles were purified by dialysis against Milli-Q water (MWCO: 1000 kDa) for 48 h. Polyoxazoline-modified SPION were obtained after freeze-

DOI: 10.1021/acs.biomac.7b01403
Biomacromolecules 2018, 19, 1435−1444

Scheme 1. Synthetic Pathway to Block Copolymer-Modified SPION[a]

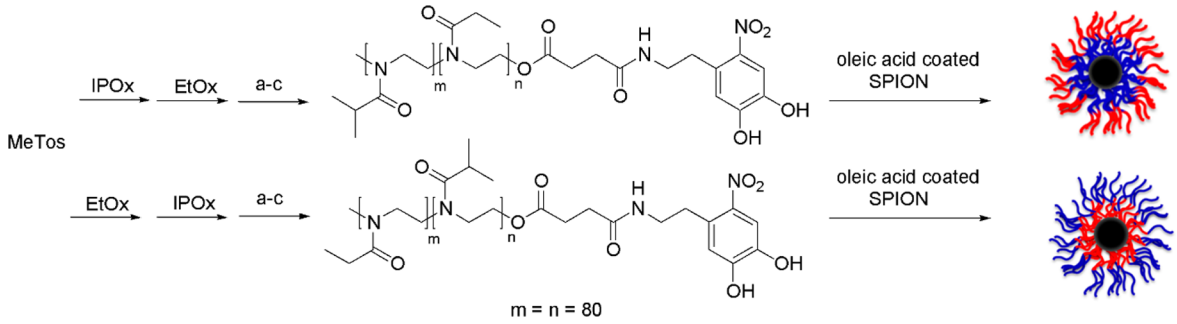

[a]MeTos: methyl tosylate, IPOx: 2-isopropyloxazoline, EtOx: 2-ethyloxazoline. (a–c) End group transformation: (a) quench with water, (b) reaction with succinic anhydride, (c) reaction with 6-nitrodopamine, ligand exchange reaction of NDA-modified block copolymers on oleic acid-coated SPION.

drying as a brown solid. FTIR (cm^{-1}): 2972 (w), 2931 (w), 2875 (w), 2853 (w), 1634 (s), 1544 (w), 1470 (s), 1426 (s), 1201 (s), 1158 (s), 1085 (m), 1061 (m), 582 (s).

Analytics. ^1H NMR spectra of polymers were measured on a BRUKER AV III 600 spectrometer. Chemical shifts were recorded in ppm and referenced to residual protonated solvent ($CDCl_3$: 7.26 ppm (1H)). Polyoxazoline molecular weights were measured by gel permeation chromatography (GPC) on an adapted Dionex HPLC utilized with a P680 HPLC pump, an ASI-100 autosampler, and an STH585 column oven. The GPC setup consists of three MZ Gel SDPlus columns (a precolumn followed by two columns with separation ranges of 10–2000 kDa and 1–40 kDa, respectively). As detector, a Knauer Smartline RI Detector 2300 was applied. As eluent, DMF with LiBr (0.05 M) was used. Samples with a concentration of 3 mg mL^{-1} were injected and measured at 60 °C with a flow rate of 0.8 mL min^{-1}. Chromeleon 6.80 with the extension pack V02 was used for analysis. Narrow dispersed polystyrene standards of 1.5–651 kg mol^{-1} were used for external calibration. Transmission electron micrographs (TEM) were recorded on an FEI Tecnai G2 with 160 kV acceleration voltage on carbon-coated grids. Nanoparticle size distributions were calculated with the freeware Pebbles[30] based on the analysis of >500 NPs. IR spectra of lyophilized samples were recorded on a Bruker Tensor 37 FTIR spectrometer at a resolution of 4 cm^{-1}, averaging 32 scans. Thermal gravimetric analysis (TGA) of the core–shell nanoparticles was performed on a Mettler Toledo TGA/DSC1 with 80 mL min^{-1} synthetic air as reactive gas, 20 mL min^{-1} nitrogen as protective gas, and a heating rate of 10 K min^{-1} from 25 to 650 °C. Mass loss from 200 to 500 °C was assigned to the polyoxazoline-NDA shell, and residual mass was assigned to the inorganic core. Mass loss up to 200 °C is due to moisture or solvent residues. Grafting density was calculated from the weight fractions by TGA, the molecular weight of the block copolymer by GPC, the average iron oxide core surface determined by TEM, and a core density of 5.18 g cm^{-3}. Dynamic light scattering (DLS) measurements (hydrodynamic diameter, scattering intensity, and temperature cycling experiments) were conducted on a Malvern Zetasizer Nano-ZS. Mean values and standard deviation (count rate and number-sized diameter) were calculated from three runs. To compare the values of the hydrodynamic diameter of the samples before and after the transition temperature, a Mann–Whitney U test was carried out. The non-normal distributed values below and above the CST were compared with a Mann–Whitney U test with an H_0 hypothesis that the distributions of both populations are equal. Size differences for which the null hypotheses could be rejected have a significance level of at least 95%. Samples were dissolved in Milli-Q water at a concentration of 1 mg mL^{-1} and filtered with a regenerated cellulose (RC) filter (0.45 μm). DSC measurements on NP dispersions in Milli-Q water (400 μL, 1 mg mL^{-1}) were performed using a MicroCal* VP-capillary DSC system at a heating rate of 1 °C min^{-1}. Data processing was done using the MicroCal VP-Capillary DSC Automated data analysis for Origin software. Enthalpy calculations are based on the mass fraction of polyoxazoline block copolymer in the material, as determined by TGA, the molecular weight of polyoxazoline block copolymer as determined by GPC, and the copolymer composition by NMR.

RESULTS AND DISCUSSION

Synthesis. The block copolymer-modified SPION were prepared by a grafting-to approach (Scheme 1), analogously to previous grafting of nitrocatechol-functionalized PEG,[27,28] PNIPAM,[3,12] and polyoxazolines[13] to SPION. The polyoxazoline block copolymers were synthesized by sequential polymerization of 2-isopropyloxazoline (IPOx) and 2-ethyloxazoline (EtOx) or by inverse order to investigate the impact of position of the individual blocks in the grafted spherical brush on the thermally induced polymer desolvation and colloidal aggregation transitions. Quenching with water generated hydroxyl-terminated polymers that were further modified by esterification with succinic anhydride and subsequent amidation with nitrodopamine to generate nitrocatechol-terminated block copolymers. Nitrodopamine has been demonstrated to be a stable anchor for grafting of polymers to SPION that are subject to harsh and destabilizing temperature cycling.[28,31,32]

Molecular weight analysis by GPC was performed before the addition of the second monomer and at the end of the block copolymerization. For both block copolymers, the molecular weight nearly doubled after polymerization of the second monomer, showing successful polymerization and chain extension (Table 1). Small low and high molecular weight shoulders were observed for both block copolymers (Figure S1). These shoulders indicate a low fraction of coupled products and dead chains of the first block.[33] These side-products cannot be end-functionalized. Thus, they will not bind to the nanoparticle surface and are removed by purification after the nanoparticle modification. Presence of the nitro-

Table 1. Characteristics of Polyoxazoline Block Copolymers

	GPC					
sample	M_n (1st block)	M_n (BCP)	PDI	target M_n (BCP)	feed mol % IPOx/ EtOx	mol % PIPOx/ PEtOx BCP (NMR)
HO-PEtOx-*b*-PIPOx	9.8	19.4	1.2	17.0	50/50	45/55
HO-PIPOx-*b*-PEtOx	10.8	19.0	1.2	17.0	50/50	48/52

DOI: 10.1021/acs.biomac.7b01403
Biomacromolecules 2018, 19, 1435–1444

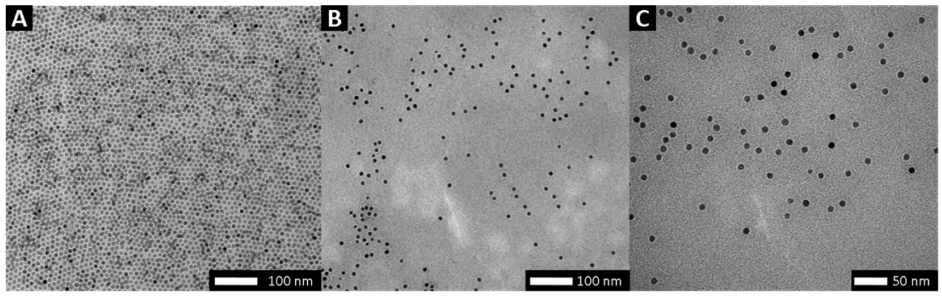

Figure 1. Transmission electron micrographs for (A) oleic acid-coated SPION, (B) FeOx@PIPOx-*b*-PEtOx, and (C) FeOx@PEtOx-*b*-PIPOx SPION grafted with nitrodopamine-functionalized block copolymers.

catechol end-group for anchoring the linear polymer to the nanoparticle surface could be confirmed by NMR spectroscopy with the aromatic resonances at 7.61 and 6.74 ppm (Figure S2).

Monodisperse, oleic acid-coated SPION with a diameter of 9.8 ± 0.6 nm were prepared by thermal decomposition of iron(0)pentacarbonyl in dioctyl ether in the presence of oleic acid (Figure 1A).[27,34] The washed oleic acid-coated SPION were then reacted with a large excess of nitrocatechol-terminated block copolymers (3 molecules nm^{-2}) in *N*,*N*-dimethylformamide (DMF) under ultrasonication to perform the ligand exchange and graft the block copolymer with high surface affinity to the nanoparticle surface. Unbound excess of the block copolymers was removed by dialysis against water (membrane cut-off: 1000 kDa). Analysis of the SPION by TGA showed grafting densities of 1.0 and 0.6 chains nm^{-2} for FeOx@PIPOx-*b*-PEtOx and FeOx@PEtOx-*b*-PIPOx, respectively (Table 2). These values are in agreement with previous

Table 2. Characteristics of SPION Grafted with Block Copolymer (FeOx@PIPOx-*b*-PEtOx and FeOx@PEtOx-*b*-PIPOx) and Free Block Copolymers

	TEM	TGA			DLS	
sample	core-D [nm]	org. loss [wt %]	residue [wt %]	σ^a [M/nm^2]	CST (PIPOx) [°C]	CST (PEtOx) [°C]
HO-PEtOx-*b*-PIPOx					55	≥100
FeOx@PEtOx-*b*-PIPOx	9.8 ± 0.6	67.7	30.3	0.6	48	86
HO-PIPOx-*b*-PEtOx					55	≥100
FeOx@PIPOx-*b*-PEtOx	9.8 ± 0.6	77.1	21.4	1.0	42.5	89

[a]Grafting density.

ligand exchange reactions with hydrophilic polymers such as PEG,[27,28] PNIPAM,[3,12] or polyoxazolines[13] performed in our group. TEM investigation of the aqueous dispersions showed dispersed nanoparticle cores with core−core distances that exceed distances observed for oleic acid-coated SPION (Figure 1B, C).

Thermal Aggregation of Block Copolymer-Modified SPION Investigated by Dynamic Light Scattering. For comparing the thermally induced aggregation of the polyoxazoline block copolymers with their nanoparticle-grafted analogues, solutions of hydroxy-terminated block copolymers and dispersions of the block copolymer-modified SPION were measured by dynamic light scattering (DLS) in the temperature range of 20−90 °C at a concentration of 1 mg mL^{-1} (0.1 wt %) in Milli-Q. As polymer coils or polymer-grafted nanoparticles reach the CST at the tested concentration, they are expected to reduce their size due to desolvation and possibly to aggregate. Changes in polymer coil and core−shell particle size can be recorded as changes in hydrodynamic diameter and in scattering intensity (count rate). The latter is very sensitive to size and aggregation and both can be monitored by DLS as a function of temperature to find the CST of a sample as when a significant change in size and/or count rate occurs.

Both the free-coil block copolymer samples show aggregation upon heating with aggregate sizes of 1.3 μm and ∼400 nm for HO-PIPOx-*b*-PEtOx and HO-PEtOx-*b*-PIPOx, respectively (Figure S5). In the chosen temperature range, only one transition for the doubly thermoresponsive block copolymers is visible. Although the aggregate cluster sizes were significantly different, the same CST of approximately 55 °C was obtained from the hydrodynamic size vs temperature DLS curves (Figure S5). This transition can be assigned to the PIPOx-block, which is expected to have a much lower CST than PEtOx. The CST of the PEtOx-block cannot be measured at this concentration but has been estimated to be ∼100 °C in Milli-Q,[13] whereas the maximum temperature that can be reached in the DLS setup is 92 °C.

The SPION grafted with block copolymer were tested under the same conditions (Figure 2). For sample FeOx@PEtOx-*b*-PIPOx, two transitions are visible in the count rate and hydrodynamic size vs temperature DLS measurements (Figure 2A, B). These can be assigned to the CST transitions of the individual blocks. The first transition occurs at 48 °C for the PIPOx-block and is rather broad, extending over 10 degrees. The transition is observed as a small increase in count rate as well as the average particle/cluster size going from 28 ± 3 to 38 ± 2 nm (Figure 2B). This increase in size was shown to be statistically significant using the null hypothesis of the Mann−Whitney U test. When comparing the aggregate size to the size below the PIPOx CST, one should keep in mind that dehydration of the shell leads to core−shell particles of smaller diameter that aggregate to clusters. We therefore measure the net result of two simultaneous processes, where one leads to reduction in average (particle) size and one leads to increase in average (cluster) size. It is, however, clear that the collapse of the outer block does not lead to strong aggregation into nanoparticle clusters or micellar structures, as the measured hydrodynamic size stays constant almost until the second transition at 86 °C upon which the core−shell nanoparticles precipitate. The precipitation can be detected by eye and which gives rise to a strong decrease in count rate followed by a loss of

DOI: 10.1021/acs.biomac.7b01403
Biomacromolecules 2018, 19, 1435−1444

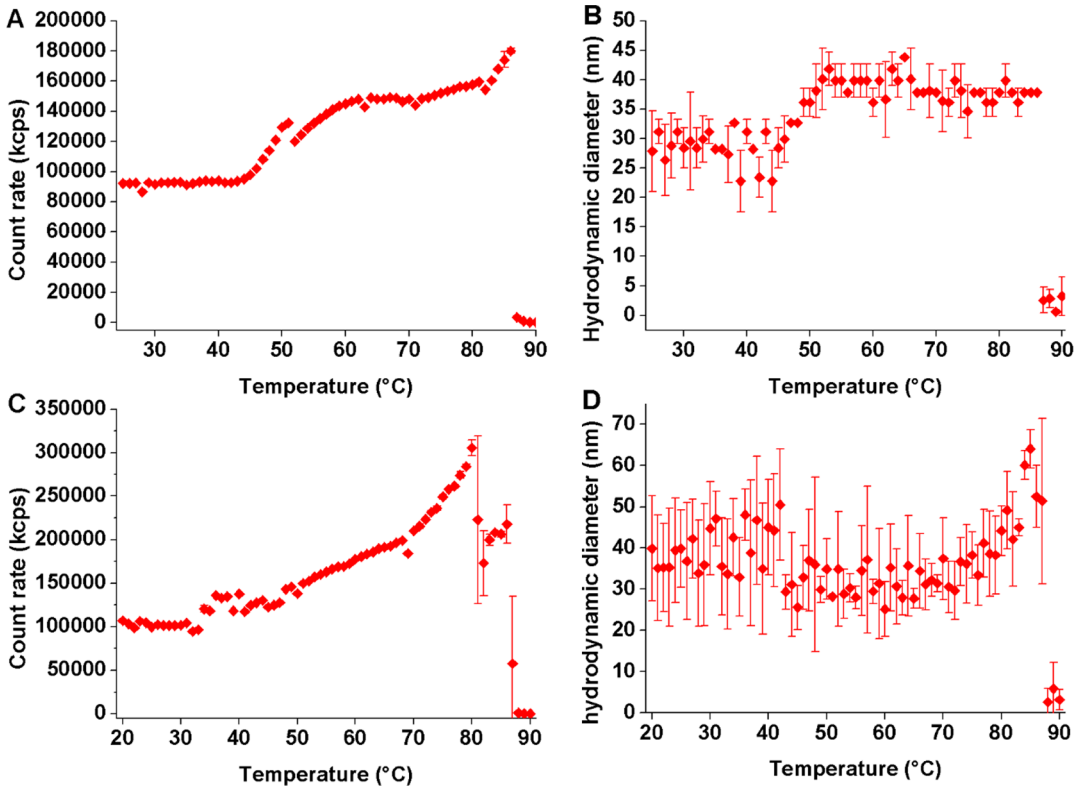

Figure 2. DLS heating curves for block copolymer-modified SPION in Milli-Q (1 mg mL^{-1}). Count rate (A) and (B) size vs temperature for FeOx@PEtOx-*b*-PIPOx, and count rate (C) and size (D) vs temperature for FeOx@PIPOx-*b*-PEtOx, mean values, and standard deviations from three measurements.

measurable sample size. At this stage, the nanoparticles can be easily extracted and decanted with a static magnet, showing that there is indeed a strong aggregation of multiple superparamagnetic cores in each cluster.

Similarly, FeOx@PIPOx-*b*-PEtOx displays two transitions (Figure 2C, D). A transition corresponding to a decrease in size is observed quite sharply at 42.5 °C and can be attributed to the PIPOx-block. Averaging the size values from 20 to 42 °C and 43 to 66 °C, one can estimate that the size decreases from 39 ± 5 to 32 ± 4 nm. This statistically significant decrease in the size by approximately 7 nm is a result of the collapse of the inner block. The first transition cannot be distinctly discerned from the count rate, which seems to exhibit a small transition already at approximately 32 °C and then starts to increase monotonously after 43 °C until the transition of the PEtOx-block. The sudden drop in count rate at 80 °C is attributed to clustering that leads to precipitation of part of the sample, leading to a loss of scattering intensity and decrease of the average size of particles remaining in the probed volume. The transition of the PEtOx-block takes place close to 89 °C and leads to a further dramatic increase in cluster size that causes rapid precipitation of the dispersion.

The hydrodynamic size measured by DLS for the fully swollen polymer shell at room temperature is larger (39 nm) for FeOx@PIPOx-*b*-PEtOx than for FeOx@PEtOx-*b*-PIPOx (28 nm). This can have two explanations: the FeOx@PIPOx-*b*-PEtOx have a higher grafting density that forces the polymer coil into a more extended brush conformation or the dense grafting close to the core makes the volume per monomer more similar for IPOx and EtOx in the inner part of the shell than in the outer part of the shell where the higher solvation of EtOx makes it expand more. Although both effects can be at play to explain the large difference, the first suggestion is likely to be the major contribution. A possible explanation for the higher grafting density obtained for nitrodopamine-terminated PIPOx-*b*-PEtOx is that the PEtOx-block, being more polar, is better solvated in the ligand exchange reaction compared to that of the PIPOx-block. Having the most expanded block closest to the core during grafting will result in a lower maximal grafting density that can be achieved for FeOx@PEtOx-*b*-PIPOx compared to for FeOx@PIPOx-*b*-PEtOx because the grafting density of polymers by ligand replacement for polymers in this size regime is limited by the solvated polymer coil size.[28]

The difference in the aggregate size above the CST that is observed with respect to block order could also tentatively be explained by the difference in exposure of the desolvated block. The particles aggregate and become larger clusters only when the stickier desolvated block is the outermost. However, it should be noted that the increase in average size is marginal, and hence the aggregates formed upon desolvation of only the PIPOx-block consist of clusters of only a few nanoparticles.

By comparing the DLS results for the *T*-scans of the two SPION samples, it is obvious that the transition temperature is influenced by the block order. Moving the PIPOx-block into closer proximity to the core results in a large decrease of the CST from 48 to 42.5 °C. The same trend is observed for the PEtOx-block with a decrease of the CST from 89 to 86 °C. The transition temperature for the grafted block copolymer decreases compared to that of the free block copolymers with a drop of 12.5 °C for the PIPOx-block close to the core and 7 °C for the PIPOx-block in the outer shell. Analogously, the PEtOx-block exhibits a drop of ∼14 and ∼11 °C for the inner and outer blocks, respectively. This reduction in transition temperature upon grafting is in agreement with reports on

DOI: 10.1021/acs.biomac.7b01403
Biomacromolecules 2018, 19, 1435−1444

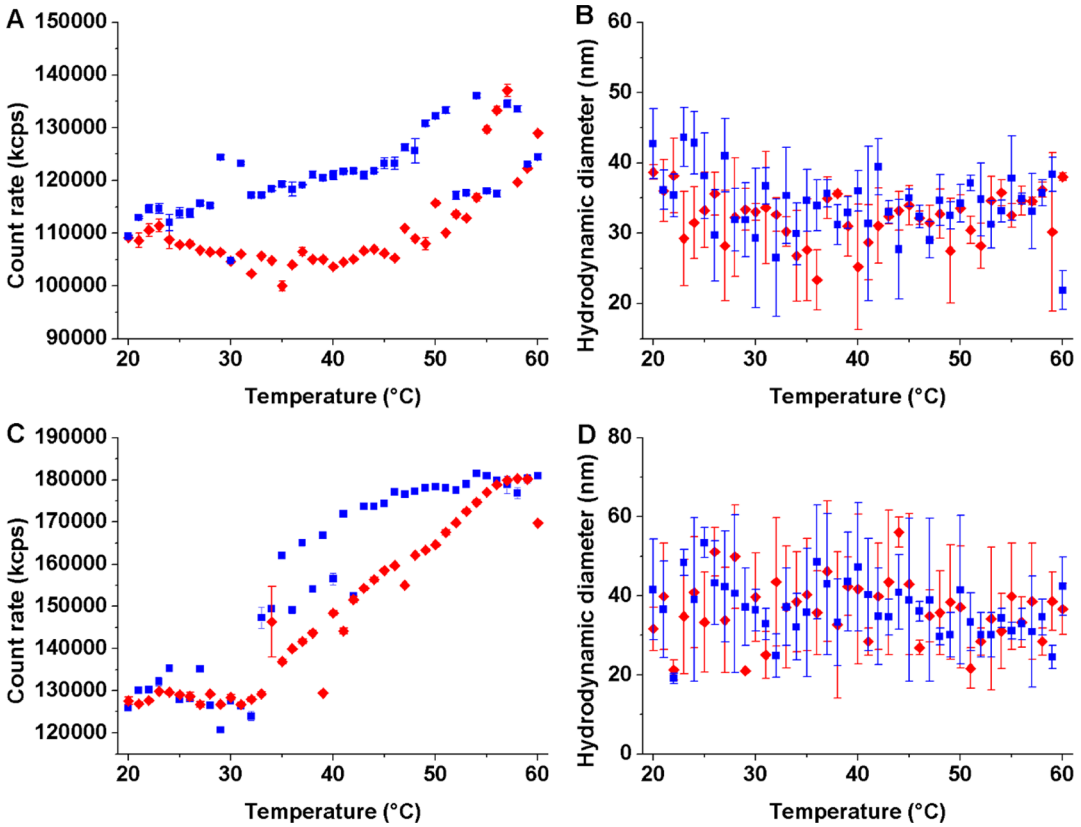

Figure 3. *T*-cycled DLS for dispersion of block copolymer-modified SPION in Milli-Q (1 mg mL^{-1}). Count rate vs temperature and size vs temperature for FeOx@PEtOx-*b*-PIPOx (A and B) and FeOx@PIPOx-*b*-PEtOx (C and D), heating curve (red diamonds), cooling curve (blue squares), mean values, and standard deviations from three measurements.

thermoresponsive polymer brushes such as polyoxazolines,[13,14] polypeptoids,[4] and poly(poly(ethylene glycol) methacrylate)[15] that all have shown a significant reduction in critical solution temperature upon grafting. A straightforward, phenomenological interpretation of this observation is that the highly hydrated polymers are above the concentration corresponding to the LCST in the phase diagram already as free coils; when they are effectively forced to even higher local concentration in a brushlike shell grafted on a nanoparticle, the critical solution temperature will drop in the phase diagram. A denser shell results in a larger decrease in CST as observed in the lower transition temperatures for the inner parts of the shell demonstrated here. Extrapolating this finding back to an extended homopolymer shell, we can expect a broadening of the transition as different parts of the shell experience different local segment densities and hence are in different parts of the phase diagram.

Heating of the SPION dispersions above the CST of the PEtOx-block leads to precipitation of both types of SPION. The precipitation was not reversible upon cooling within the experimental time frame. The aggregated samples could be redispersed over longer time scales or by sonication, whereupon they showed the same colloidal stability as before. Thus, clustering was due to aggregation of the shells and not by thermally induced loss of grafted polymer chains from the shell. To be able to investigate reversible aggregation and deaggregation with spontaneous redispersion during a single DLS temperature run, we next performed *T*-cycled DLS experiments only below the transition of the PEtOx-block in the temperature range 20−60 °C. In this range, only the solubility transition of the PIPOx-block is probed. For FeOx@PEtOx-*b*-PIPOx, the count rate is reversible, returning to the initial values (Figure 3A). The count rate increases in agreement with previous measurements at approximately 48 °C. However, the size curve for the sample lacks a clear transition point. The size stays almost constant with only a small increase in average particle size of ∼2 nm from 31 ± 3 to 33 ± 3 nm above 47 °C. This small size change was in contrast to the larger increase in size of ∼10 nm observed for the heating curves recorded for the full temperature range in Figure 2 not statistically significant. Sample FeOx@PIPOx-*b*-PEtOx displays a reversible count rate (Figure 3C) within the limited temperature range just as FeOx@PEtOx-*b*-PIPOx. For both samples, a slight hysteresis in part of the count rate curves is observed (Figure 3A and C), which is absent from the size curves. The absence of hysteresis for PIPOx in both types of SPION grafted with block copolymer is a clear indication of fast rehydration of the polymer; cooling to temperatures far below the CST as observed for some other thermoresponsive polymers[35] was not required. Similar observations of fast rehydration and deaggregation were made for SPION grafted with a PIPOx homopolymer brush (MW: 16.5 kDa),[13] but it contrasts with SPION grafted with the isomeric PNIPAM (MW: 20 kDa) that exhibited strong hysteresis upon cooling.[3] The faster rehydration kinetics for PIPOx in comparison to PNIPAM could be explained by the overall lower hydrogen bonding capacity of PIPOx, which has been described as leading to faster rehydration of PIPOx upon cooling by van Mele and co-workers.[35]

DOI: 10.1021/acs.biomac.7b01403
Biomacromolecules 2018, 19, 1435−1444

The size curve for FeOx@PIPOx-*b*-PEtOx (Figure 3D) exhibits a drop in average hydrodynamic diameter at ~43−44 °C, as observed for the larger temperature range cycling. Averaging the values before and after 43 °C shows that the size decreases from 38 ± 7 to 33 ± 5 by approximately 5 nm. This decrease is comparable to the 7 nm decrease determined from the data for the larger temperature range presented in Figure 2D, but due to the higher variability in the cycled measurements, this 5 nm decrease did not reach the same high level of statistical significance. Thus, although quite noisy, the collapse of the inner block leads again to a lower hydrodynamic size with no observed aggregation. The change is fully reversible upon cooling. Given the small measured changes in the hydrodynamic size of SPION grafted with thermoresponsive block copolymer upon heating, it is obvious that monitoring these processes by DLS is at its limit. Given that the count rate increases, we cannot rule out that some aggregation also occurs that partially masks the decrease in average nanoparticle size. For future investigations, an increase in the block molecular weights and thus brush thickness could help to sharpen the transitions.[26]

Summarizing the results from measuring *T*-cycled changes in light scattering and hydrodynamic diameter, grafting of thermoresponsive polymer chains has a strong impact on their transition temperature, which is more pronounced for the polymer segments close to the core. This result can be explained by the varying chain segment density throughout the brush with regimes that differ in their hydration state and in their effective concentration and therefore place in the phase diagram. Indeed, investigations by SAXS on SPION melt-grafted with PEG to extremely dense spherical brush shells have shown distinct density profile regimes as a function of distance from the iron oxide core surface.[36] A very strong influence of the grafted polymer molecular weight on the thermoresponsive aggregation behavior of nanoparticles that has been observed[3,12,13] could also be partially due to the different fractions of those polymers that are in a dense brush regime in a near-free coil or mushroom regime. Interestingly, aggregate sizes for the free block copolymers surpass those of SPION grafted with the same polymer by 1 order of magnitude. This difference in the aggregation behavior might be linked to differences in the transition enthalpy.

Investigation of the Transition Enthalpy by DSC. For further insights into the impact of grafting and the position of the blocks on the thermoresponsive properties, solutions of free block copolymers and dispersions of SPION grafted with block copolymer were investigated by DSC in a temperature range of 20−90 °C at the same mass concentration of 1 mg mL^{-1} (Table 3, Figure 4). In both block copolymers, the PIPOx-block has a molecular weight of ~9.5 kDa, making a direct comparison between the two kinds of modified nanoparticles and the free polymers possible. For all samples, a single endothermic peak is observed, even for the block copolymer-modified SPION. This transition is assigned to the thermally driven desolvation of the PIPOx-block. Although the transition of the PEtOx-block, as shown by DLS, is occurring within the investigated temperature range, no second heat peak is observed before 90 °C is reached. This observation is in agreement with DSC measurements on SPION grafted with PEtOx homopolymers (14 kDa, CST of ~74 °C in Milli-Q), which also did not display a visible peak in the same temperature range.[13]

Table 3. DSC Results for Free Block Copolymers and SPION Grafted with Block Copolymer

sample	M_n PIPOx-block [g moL^{-1}][a]	ΔH PIPOx-block [J g^{-1}][b]	ΔH [kJ (mol RU)$^{-1}$]	T_{onset} [°C]	T_{peak} [°C]	FWHM [°C]
HO-PEtOx-*b*-PIPOx	9747	48.96	5.54	50.90	62.90	11.66
FeOx@PEtOx-*b*-PIPOx	9747	7.37	0.83	39.70	50.90	8.50
HO-PIPOx-*b*-PEtOx	9367	56.54	6.39	52.00	61.00	11.32
FeOx@PIPOx-*b*-PEtOx	9367	5.15	0.58	30.10	32.60	0.40

[a]MW of PIPOx calculated from BCP-molecular weight (GPC) and copolymer composition by NMR. [b]Transition enthalpy for the poly(2-isopropyloxazoline)-block.

For each of the precursor polymers, a single yet broad transition peak is measured with peak temperatures of 62.9 °C for HO-PEtOx-*b*-PIPOx and 61 °C for HO-PIPOx-*b*-PEtOx, respectively (Figure 4A, C). Thus, quite comparable transition temperatures are obtained for the free block copolymers independent of the block order. However, the transition temperatures for the PIPOx-block are reduced after grafting with temperatures of 50.9 °C for FeOx@PEtOx-*b*-PIPOx and even 32.6 °C for FeOx@PIPOx-*b*-PEtOx (Figure 4B, D). Thus, the block order in the spherical brush has a dramatic effect on the transition temperature, showing that polymer segments close to the core are highly affected in their thermoresponsive properties with a drop in transition temperature of 28 °C, as measured for FeOx@PIPOx-*b*-PEtOx. Placing the PIPOx-block in the outer segment reduces the effect of grafting on the transition temperature, but still results in a reduction by 12 °C. The onset temperatures by DSC for the free polymers and for the SPION grafted with block copolymer are lower compared to values obtained by DLS. The onset of the transition temperature measured for FeOx@PIPOx-*b*-PEtOx fits to the small transition in count rate at 32 °C observed by DLS (Figures 2C and 3C) and not to the pronounced reduction in size observed at 43 °C (Figure 2D). Although the different heating rates of DSC and DLS might have an influence on the transition temperature, this trend indicates that dehydration takes place before the major conformational change and reduction in brush size occurs.

Another interesting observation is that the peak half-width of the grafted PIPOx-block is highly dependent on the morphology of the polymer and in particular on whether it is grafted in the dense proximity of the core. In case the PIPOx is kept as outer block, only a 30% reduction in the peak half width is observed by grafting as a brush to the SPION core (Figure 4A and B, Table 3). Moving the PIPOx-block close to the core results in a tremendous sharpening of the transition peak compared to the free block copolymer with peak width being only 3.5% of the free polymer peak width (Figure 4C and D, Table 3). A plausible explanation for this effect in line with the interpretation of the shifts in transition temperature measured by DSC and DLS is that the outer PIPOx-block displays similar behavior to a free polymer chain, hardly interacting with neighboring PIPOx-chains, whereas the inner PIPOx-block in

DOI: 10.1021/acs.biomac.7b01403
Biomacromolecules 2018, 19, 1435−1444

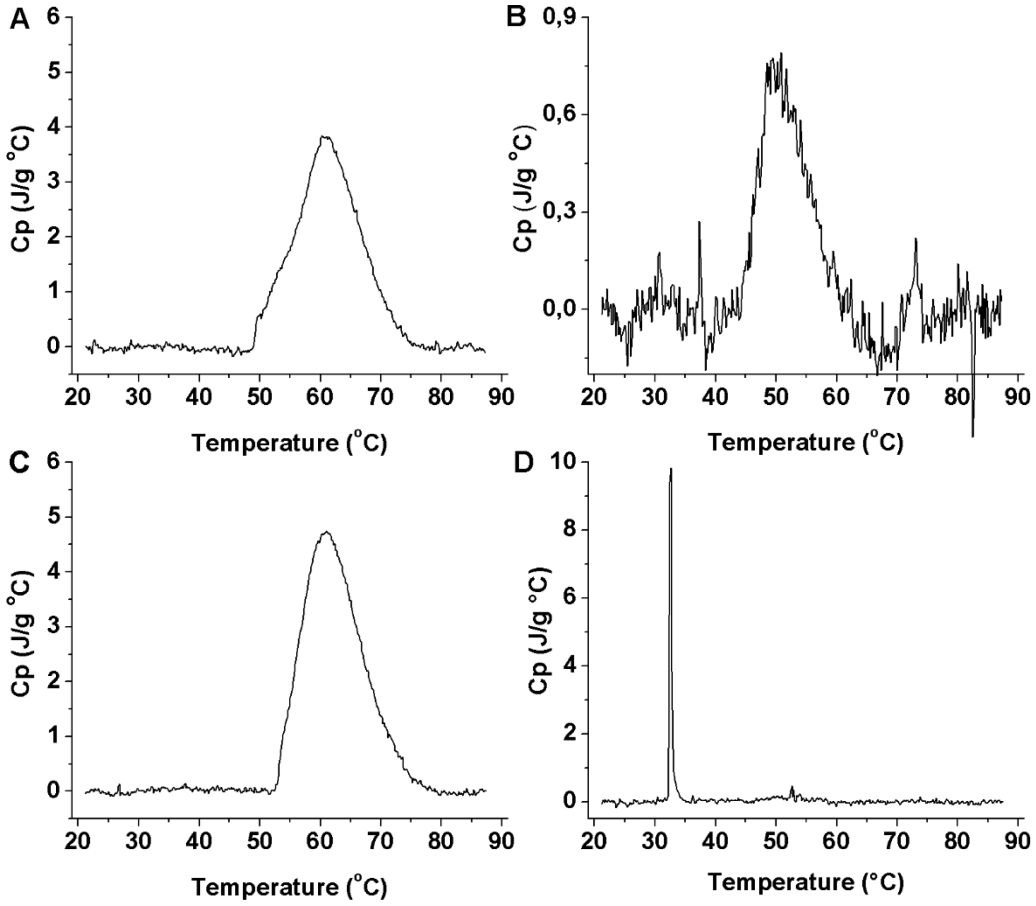

Figure 4. DSC heating curves for solutions of block copolymers HO-PEtOx-*b*-PIPOx (A) and HO-PIPOx-*b*-PEtOx (C) and dispersions of block copolymer-grafted SPION FeOx@PEtOx-*b*-PIPOx (B) and FeOx@PIPOx-*b*-PEtOx (D) in Milli-Q-water, concentration of 1 mg mL^{-1}, heating rate 1 K min^{-1}, 20 to 90 °C, curves normalized on MW of the individual PIPOx-blocks.

its confined geometry of a melt-like chain density[36] dehydrates in a concerted, codependent fashion.

The transition enthalpy is also strongly affected by the grafting process.[12,13] The free block copolymers display transition enthalpies of 5.5−6.4 kJ (mol repeating unit)$^{-1}$, which are equal to breaking of one hydrogen bond per repeating unit.[37] After grafting, the enthalpies are strongly reduced to values of 0.83 and 0.58 kJ (mol repeating unit)$^{-1}$ for FeOx@PEtOx-*b*-PIPOx and FeOx@PIPOx-*b*-PEtOx, respectively. Thus, the transition enthalpy is significantly lowered after grafting, which is more pronounced for the PIPOx-block close to the core (FeOx@PIPOx-*b*-PEtOx) compared to the polymer segments in the outer shell (FeOx@PEtOx-*b*-PIPOx). Still, the outer segments of the spherical brush also experience a drastic reduction in transition enthalpy, indicating that these segments are far from the hydration state of a free polymer coil. This indicates that most of the outer part of the polymer shell is also in a brush rather than mushroom state. It can be assumed that this effect can be weakened by further distancing the PIPOx-block from the core. The smaller number of hydrogen bonds being broken for grafted PIPOx suggests that they also collapse to a lower extent than free polymers. This is assumed to be the main reason for the low aggregate size of grafted SPION compared to free polymer coils observed by DLS. A recent study on SPION grafted with PNIPAM showed that the aggregate size is highly affected by the dispersant molecular weight. Thus, extension of the thermoresponsive blocks could lead to larger aggregate sizes.[12]

These results show that DLS and DSC are complementary techniques to investigate temperature-triggered solubility transitions of nanoparticles. Although DSC measures changes in enthalpy mirroring the breaking of polymer−water hydrogen bonds, DLS measures changes in hydrodynamic size, allowing for monitoring swelling of the shell and aggregation of thermoresponsive SPION.

CONCLUSIONS

Two polyoxazoline block copolymers functionalized with nitrodopamine were used for the preparation of core−shell SPION with shells having two distinct solubility transition temperatures of the shell. The combined results of determining transition temperatures by DLS and DSC and transition enthalpy by DSC clearly show the strong impact of the grafting process on the thermoresponsive properties of the polymer. We demonstrate that this effect is not uniformly imposed throughout the shell but much stronger (lower CST, narrower and smaller endothermic peak of the transition) close to the particle core where the polymer segment density is very high. Clearly, the evidence is strong for different regimes in a spherical brush being characterized by different hydration states as well as different interactions with the core and neighboring chains. The outer segments experience less sterical crowding, but nonetheless, a significant reduction of their responsiveness is observed as a result of the grafting.

Furthermore, the aggregation of SPION grafted with block copolymer leads to significantly smaller clusters than for the

DOI: 10.1021/acs.biomac.7b01403
Biomacromolecules 2018, 19, 1435−1444

equivalent free coil block copolymers despite the effectively higher molecular weight of the grafted nanoparticles than of the free coils. The steric repulsion and reduced interpenetration of polymers in the nanoparticle shells therefore seem to outweigh the molecular weight effect previously observed to lead to larger aggregates for higher molecular weight polymers.

SPION grafted with block copolymer can be thermally switched in two steps, although heating above the critical solution temperature of the PEtOx-block results in strong aggregation that hinders redispersion. Further tuning of the composition and molecular weight of the blocks could thereby possibly be used to reversibly alternate between multiple particle hydrodynamic sizes and colloidal aggregation states. In future studies, we will therefore aim to create shells that from structure and composition allow us to magnetically control thermal change of size and aggregation state without affecting the bulk water temperature, something that has previously proven elusive due to either overall compromised colloidal stability or too fast heat diffusion through the shell to allow thermal switching of the shell. Such exquisite all-magnetic control over functionality and aggregation could be used to realize new extraction and purification schemes for biotechnological separation as well as medical imaging and hyperthermia applications.

■ ASSOCIATED CONTENT

Supporting Information

The Supporting Information is available free of charge on the ACS Publications website at DOI: 10.1021/acs.biomac.7b01403.

^{1}H NMR spectra, GPC and DLS heating curves of free block copolymers, TGA curves and FTIR spectra of block copolymer-modified SPION, and an example of calculations of the copolymer grafting density on SPION (PDF)

■ AUTHOR INFORMATION

Corresponding Author

*E-mail: erik.reimhult@boku.ac.at. Tel: +43 1 47654 80211. Fax: +43 1 47891 12.

ORCID

Erik Reimhult: 0000-0003-1417-5576

Present Address

†S.K.: AIT Austrian Institute of Technology GmbH, Center for Health & Bioresources, Molecular Diagnostics, Donau-City-Straße 1, 1220 Vienna, Austria

Author Contributions

S.K., R.Z., and E.R. planned the work. S.K. conducted and evaluated all experiments except DSC measurements conducted by N.G. M.S. synthesized 2-isopropyloxazoline. S.K. and E.R. wrote the manuscript. All authors reviewed the manuscript.

Notes

The authors declare no competing financial interest.

■ ACKNOWLEDGMENTS

The research leading to these results was funded by the European Research Council under the European Union's Seventh Framework Program (FP/2007-2013)/ERC Grant Agreement no. 310034 and the Austrian Science Fund (FWF) project P 28190-N28. We acknowledge the VIBT Extremophile Center for access to TGA.

■ REFERENCES

(1) Gibson, M. I.; O'Reilly, R. K. To aggregate, or not to aggregate? considerations in the design and application of polymeric thermally-responsive nanoparticles. *Chem. Soc. Rev.* **2013**, *42* (17), 7204−7213.

(2) Yildiz, I.; Sizirici Yildiz, B. Applications of Thermoresponsive Magnetic Nanoparticles. *J. Nanomater.* **2015**, *2015*, 12.

(3) Kurzhals, S.; Zirbs, R.; Reimhult, E. Synthesis and Magneto-Thermal Actuation of Iron Oxide Core−PNIPAM Shell Nanoparticles. *ACS Appl. Mater. Interfaces* **2015**, *7* (34), 19342−19352.

(4) Kurzhals, S.; Pretzner, B.; Reimhult, E.; Zirbs, R. Thermoresponsive polypeptoid-coated superparamagnetic iron oxide nanoparticles by surface-initiated polymerization. *Macromol. Chem. Phys.* **2017**, *218* (13), 1700116.

(5) Zhao, Q.; Chen, N.; Zhao, D.; Lu, X. Thermoresponsive Magnetic Nanoparticles for Seawater Desalination. *ACS Appl. Mater. Interfaces* **2013**, *5* (21), 11453−11461.

(6) Hannecart, A.; Stanicki, D.; Vander Elst, L.; Muller, R. N.; Lecommandoux, S.; Thevenot, J.; Bonduelle, C.; Trotier, A.; Massot, P.; Miraux, S.; Sandre, O.; Laurent, S. Nano-thermometers with thermo-sensitive polymer grafted USPIOs behaving as positive contrast agents in low-field MRI. *Nanoscale* **2015**, *7* (8), 3754−3767.

(7) Wang, Z.; Ma, X.; Zong, S.; Wang, Y.; Chen, H.; Cui, Y. Preparation of a magnetofluorescent nano-thermometer and its targeted temperature sensing applications in living cells. *Talanta* **2015**, *131*, 259−265.

(8) Zeltner, M.; Schatz, A.; Hefti, M. L.; Stark, W. J. Magneto-thermally responsive C/Co@PNIPAM-nanoparticles enable preparation of self-separating phase-switching palladium catalysts. *J. Mater. Chem.* **2011**, *21* (9), 2991−2996.

(9) Allam, A. A.; Sadat, M. E.; Potter, S. J.; Mast, D. B.; Mohamed, D. F.; Habib, F. S.; Pauletti, G. M. Stability and magnetically induced heating behavior of lipid-coated Fe_3O_4 nanoparticles. *Nanoscale Res. Lett.* **2013**, *8* (1), 426−426.

(10) Pernia Leal, M.; Torti, A.; Riedinger, A.; La Fleur, R.; Petti, D.; Cingolani, R.; Bertacco, R.; Pellegrino, T. Controlled Release of Doxorubicin Loaded within Magnetic Thermo-responsive Nanocarriers under Magnetic and Thermal Actuation in a Microfluidic Channel. *ACS Nano* **2012**, *6* (12), 10535−10545.

(11) Jaiswal, M. K.; De, M.; Chou, S. S.; Vasavada, S.; Bleher, R.; Prasad, P. V.; Bahadur, D.; Dravid, V. P. Thermoresponsive Magnetic Hydrogels as Theranostic Nanoconstructs. *ACS Appl. Mater. Interfaces* **2014**, *6* (9), 6237−6247.

(12) Kurzhals, S.; Gal, N.; Zirbs, R.; Reimhult, E. Aggregation of thermoresponsive core-shell nanoparticles: influence of particle concentration, dispersant molecular weight and grafting. *J. Colloid Interface Sci.* **2017**, *500*, 321−332.

(13) Kurzhals, S.; Gal, N.; Zirbs, R.; Reimhult, E. Controlled aggregation and cell uptake of thermoresponsive polyoxazoline-grafted superparamagnetic iron oxide nanoparticles. *Nanoscale* **2017**, *9*, 2793−2805.

(14) Koshkina, O.; Lang, T.; Thiermann, R.; Docter, D.; Stauber, R. H.; Secker, C.; Schlaad, H.; Weidner, S.; Mohr, B.; Maskos, M.; Bertin, A. Temperature-Triggered Protein Adsorption on Polymer-Coated Nanoparticles in Serum. *Langmuir* **2015**, *31* (32), 8873−81.

(15) Gibson, M. I.; Paripovic, D.; Klok, H. A. Size-Dependent LCST Transitions of Polymer-Coated Gold Nanoparticles: Cooperative Aggregation and Surface Assembly. *Adv. Mater.* **2010**, *22* (42), 4721−4725.

(16) Cook, M. T.; Filippov, S. K.; Khutoryanskiy, V. V. Synthesis and solution properties of a temperature-responsive PNIPAM-b-PDMS-b-PNIPAM triblock copolymer. *Colloid Polym. Sci.* **2017**, *295* (8), 1351−1358.

(17) Luo, Y.-L.; Zhang, J.; Han, F.-J.; Xu, F.; Chen, Y.-S.; Liu, R. Epoxidized poly(N-isopropyl acrylamide)-b-epoHTPB-b-poly(N-isopropyl acrylamide) triblock copolymer micelle nanoparticles for 10-hydroxycamptothecin drug release. *J. Appl. Polym. Sci.* **2015**, *132* (18), 41877/1−41877/11.

(18) San Miguel, V.; Limer, A. J.; Haddleton, D. M.; Catalina, F.; Peinado, C. Biodegradable and thermoresponsive micelles of triblock

DOI: 10.1021/acs.biomac.7b01403
Biomacromolecules 2018, 19, 1435−1444

copolymers based on 2-(N,N-dimethylamino)ethyl methacrylate and ε-caprolactone for controlled drug delivery. *Eur. Polym. J.* **2008**, *44* (11), 3853−3863.
(19) Cao, Y.; Zhao, N.; Wu, K.; Zhu, X. X. Solution Properties of a Thermosensitive Triblock Copolymer of N-Alkyl Substituted Acrylamides. *Langmuir* **2009**, *25* (3), 1699−1704.
(20) Chen, J.; Liu, M.; Gong, H.; Huang, Y.; Chen, C. Synthesis and Self-Assembly of Thermoresponsive PEG-b-PNIPAM-b-PCL ABC Triblock Copolymer through the Combination of Atom Transfer Radical Polymerization, Ring-Opening Polymerization, and Click Chemistry. *J. Phys. Chem. B* **2011**, *115* (50), 14947−14955.
(21) Cheng, C.; Wei, H.; Zhu, J.-L.; Chang, C.; Cheng, H.; Li, C.; Cheng, S.-X.; Zhang, X.-Z.; Zhuo, R.-X. Functionalized Thermoresponsive Micelles Self-Assembled from Biotin-PEG-b-P(NIPAAm-co-HMAAm)-b-PMMA for Tumor Cell Target. *Bioconjugate Chem.* **2008**, *19* (6), 1194−1201.
(22) Li, Y.; Lokitz, B. S.; Armes, S. P.; McCormick, C. L. Synthesis of Reversible Shell Cross-Linked Micelles for Controlled Release of Bioactive Agents. *Macromolecules* **2006**, *39* (8), 2726−2728.
(23) Zhang, W.; Jiang, X.; He, Z.; Xiong, D.; Zheng, P.; An, Y.; Shi, L. Thermoresponsive core-shell-corona micelles of poly(ethylene glycol)-b-poly(N-isopropylacrylamide)-b-polystyrene. *Polymer* **2006**, *47* (24), 8203−8209.
(24) Li, Q.; Huo, F.; Cui, Y.; Gao, C.; Li, S.; Zhang, W. Doubly thermoresponsive brush-linear-linear ABC triblock copolymer nanoparticles prepared through dispersion RAFT polymerization. *J. Polym. Sci., Part A: Polym. Chem.* **2014**, *52* (16), 2266−2278.
(25) Eyiler, E.; Walters, K. B. Magnetic iron oxide nanoparticles grafted with poly(itaconic acid)-block-poly(N-isopropylacrylamide). *Colloids Surf., A* **2014**, *444*, 321−325.
(26) Tang, T.; Krysmann, M. J.; Hamley, I. W. In situ formation of gold nanoparticles with a thermo-responsive block copolymer corona. *Colloids Surf., A* **2008**, *317* (1−3), 764−767.
(27) Lassenberger, A.; Bixner, O.; Grünewald, T. A.; Lichtenegger, H. C.; Zirbs, R.; Reimhult, E. Evaluation of high-yield purification methods on monodisperse PEG-grafted iron oxide nanoparticles. *Langmuir* **2016**, *32* (17), 4259−4269.
(28) Zirbs, R.; Lassenberger, A.; Vonderhaid, I.; Kurzhals, S.; Reimhult, E. Melt-Grafting for the Synthesis of Core-Shell Nanoparticles with Ultra-High Dispersant Density. *Nanoscale* **2015**, *7*, 11216−11225.
(29) Monnery, B. D.; Shaunak, S.; Thanou, M.; Steinke, J. H. G. Improved Synthesis of Linear Poly(ethylenimine) via Low-Temperature Polymerization of 2-Isopropyl-2-oxazoline in Chlorobenzene. *Macromolecules* **2015**, *48* (10), 3197−3206.
(30) Mondini, S.; Ferretti, A. M.; Puglisi, A.; Ponti, A. Pebbles and PebbleJuggler: software for accurate, unbiased, and fast measurement and analysis of nanoparticle morphology from transmission electron microscopy (TEM) micrographs. *Nanoscale* **2012**, *4* (17), 5356−5372.
(31) Amstad, E.; Gillich, T.; Bilecka, I.; Textor, M.; Reimhult, E. Ultrastable Iron Oxide Nanoparticle Colloidal Suspensions Using Dispersants with Catechol-Derived Anchor Groups. *Nano Lett.* **2009**, *9* (12), 4042−4048.
(32) Amstad, E.; Textor, M.; Reimhult, E. Stabilization and functionalization of iron oxide nanoparticles for biomedical applications. *Nanoscale* **2011**, *3* (7), 2819−2843.
(33) Verbraeken, B.; Monnery, B. D.; Lava, K.; Hoogenboom, R. The chemistry of poly(2-oxazoline)s. *Eur. Polym. J.* **2017**, *88*, 451−469.
(34) Hyeon, T.; Lee, S. S.; Park, J.; Chung, Y.; Na, H. B. Synthesis of Highly Crystalline and Monodisperse Maghemite Nanocrystallites without a Size-Selection Process. *J. Am. Chem. Soc.* **2001**, *123* (51), 12798−12801.
(35) Zhao, J.; Hoogenboom, R.; Van Assche, G.; Van Mele, B. Demixing and Remixing Kinetics of Poly(2-isopropyl-2-oxazoline) (PIPOZ) Aqueous Solutions Studied by Modulated Temperature Differential Scanning Calorimetry. *Macromolecules* **2010**, *43* (16), 6853−6860.
(36) Grünewald, T. A.; Lassenberger, A.; van Oostrum, P. D. J.; Rennhofer, H.; Zirbs, R.; Capone, B.; Vonderhaid, I.; Amenitsch, H.; Lichtenegger, H. C.; Reimhult, E. Core−Shell Structure of Monodisperse Poly(ethylene glycol)-Grafted Iron Oxide Nanoparticles Studied by Small-Angle X-ray Scattering. *Chem. Mater.* **2015**, *27* (13), 4763−4771.
(37) Diab, C.; Akiyama, Y.; Kataoka, K.; Winnik, F. M. Microcalorimetric Study of the Temperature-Induced Phase Separation in Aqueous Solutions of Poly(2-isopropyl-2-oxazolines). *Macromolecules* **2004**, *37* (7), 2556−2562.

DOI: 10.1021/acs.biomac.7b01403
Biomacromolecules 2018, 19, 1435−1444